The Journal of Chemical Physics

RESEARCH ARTICLE | FEBRUARY 29 2024

Photo-driven water oxidation performed by supramolecular photocatalysts made of Ru(II) photosensitizers and catalysts

Special Collection: The Physical Chemistry of Solar Fuels Catalysis

Ambra M. Cancelliere ; Antonino Arrigo ; Maurilio Galletta ; Francesco Nastasi ; Sebastiano Campagna ; Giuseppina La Ganga

J. Chem. Phys. 160, 084709 (2024)
https://doi.org/10.1063/5.0189316

AIP Publishing

The Journal of Chemical Physics ARTICLE pubs.aip.org/aip/jcp

Photo-driven water oxidation performed by supramolecular photocatalysts made of Ru(II) photosensitizers and catalysts

Cite as: J. Chem. Phys. 160, 084709 (2024); doi: 10.1063/5.0189316
Submitted: 28 November 2023 • Accepted: 30 January 2024 •
Published Online: 29 February 2024

Ambra M. Cancelliere,[1] Antonino Arrigo,[1] Maurilio Galletta,[2] Francesco Nastasi,[1] Sebastiano Campagna,[1,a)] and Giuseppina La Ganga[1,a)]

AFFILIATIONS

[1] Dipartimento di Scienze Chimiche, Biologiche, Farmaceutiche e Ambientali, and Interuniversitary Research Center on Artificial Photosynthesis (SOLAR-CHEM, Messina Node), University of Messina, via F. Stagno d'Alcontres 31, 98166 Messina, Italy
[2] URT LABSENS DSFTM CNR, via F. Stagno d'Alcontres 31, 98166 Messina, Italy

Note: This paper is part of the JCP Special Topic on The Physical Chemistry of Solar Fuels Catalysis.
[a)]**Authors to whom correspondence should be addressed:** campagna@unime.it and glaganga@unime.it

ABSTRACT

Two new supramolecular photocatalysts made of covalently linked Ru(II) polypyridine chromophore subunits ($[Ru(bpy)_3]^{2+}$-type species; bpy = 2,2′-bipyridine) and $[RuL(pic)_2]$ (L = 2,2′-bipyridine-6,6′-dicarboxylic acid; pic = 4-picoline) water oxidation catalyst subunits have been prepared. The new species, **1** and **2**, contain chromophore and catalyst subunits in the molecular ratios 1:1 and 1:2, respectively. The model chromophore species $[Ru(bpy)_2(L1)]^{2+}$ (**RuP1**; L1 = 4-[2-(4-pyridyl)-2-hydroxyethyl]-4-methyl-2,2′-bipyridine) and $[Ru(bpy)_2(L2)]^{2+}$ (**RuP2**; L2 = 4,4′-bis[2-(4-pyridyl)-2-hydroxyethyl]-2,2′-bipyridine) have also been prepared. The absorption spectra, oxidation behavior, and luminescent properties of **1** and **2** have been studied, and the results indicate that each subunit largely maintains its own properties in the supramolecular species. However, the luminescence of the chromophore subunits is significantly quenched in **1** and **2** in comparison with the luminescence of the respective model species. Both **1** and **2** exhibit catalytic water oxidation in the presence of cerium ammonium nitrate, exhibiting an I2M mechanism, with a better efficiency than the known catalyst $[RuL(pic)_2]$ under the same experimental conditions. Upon light irradiation, in the presence of persulfate as a sacrificial acceptor agent, **1** and **2** are more efficient photocatalysts than a system made of separated $[Ru(bpy)_3]^{2+}$ and $[RuL(pic)_2]$ species, highlighting the advantage of using multicomponent, supramolecular species with respect to isolated species. The O–O bond formation step is I2M, even in the photo-driven process. The photocatalytic process of **2** is more efficient than that of **1**, with the turnover frequency reaching a value of 1.2 s^{-1}. A possible reason could be an increased local concentration of catalytic subunits in the needed bimolecular assembly required for the I2M mechanism in **2** with respect to **1**, a consequence of the presence of two catalytic subunits in each multicomponent species **2**.

INTRODUCTION

Photo-driven water oxidation is a bottleneck for the development of efficient artificial photosynthesis.[1] Actually, water oxidation to molecular oxygen is a quite complex reaction, and the design of synthetic assemblies capable of performing this reaction with a high quantum yield and efficiency is at the center of a large research activity.[1,2]

In recent times, supramolecular photocatalysts, made of covalently linked chromophore units (having the role of absorbing light) and molecular catalysts (having the role of running the catalytic process), have been largely explored as potential light-driven water oxidation species.[3] In such systems, the light energy absorbed by the chromophore component(s) is used, upon a series of photoinduced intercomponent electron transfer processes, to power the catalytic properties of the catalyst component(s). The advantage of such supramolecular photocatalysts compared to separated chromophore and catalyst units resides in the faster rate constant for intercomponent electron transfer processes, which do not suffer from diffusion. Obviously, important factors for the efficiency of the processes are thermodynamic and kinetic factors, with the latter largely influenced by the electronic coupling between the

subunits and, therefore, by the nature and size of the covalent connectors.[4]

Here, we report the photocatalytic water oxidation properties of two new supramolecular photocatalysts made of Ru(II) polypyridine chromophore subunits ($[Ru(bpy)_3]^{2+}$-type species; bpy = 2,2′-bipyridine) and $[RuL(pic)_2]$ (L = 2,2′-bipyridine-6,6′-dicarboxylic acid; pic = 4-picoline) catalyst subunits. The $[RuL(pic)_2]$ species is known to be a quite fast and efficient water oxidation catalyst,[5] whereas Ru(II) polypyridine complexes are standard photosensitizers for photoinduced processes, including photoinduced water oxidation, thanks to their outstanding photophysical and redox properties.[6] The structural formulas of the new multicomponent species **1** and **2** here studied, together with the chromophore components $[Ru(bpy)_2(L1)]^{2+}$ (**RuP1**; L1 = 4-[2-(4-pyridyl)-2-hydroxyethyl]-4-methyl-2,2′-bipyridine) and $[Ru(bpy)_2(L2)]^{2+}$ (**RuP2**; L2 = 4,4′-bis[2-(4-pyridyl)-2-hydroxyethyl]-2,2′-bipyridine) and the catalytic species $[RuL(pic)_2]$ (**RuC**), used as models, are shown in Fig. 1. Similar subunits have already been used to prepare supramolecular photocatalysts for water oxidation.[7,8] The species reported here differs from formerly investigated compounds also because of the different connections between the components. Moreover, the chromophore:catalyst ratio in **2** is 1:2, a never explored ratio in former supramolecular photocatalyst species for water oxidation based on Ru(II) components. We decided to explore this ratio also in light of the superior photocatalytic properties exhibited by species having a 1:2 chromophore:catalyst ratio in supramolecular photocatalysts for CO_2 photoreduction.[9]

RESULTS AND DISCUSSION

The synthetic procedure used to prepare **2** is schematized in Fig. 2. An analogous procedure has been used to prepare **1** and is reported in the supplementary material.

The absorption spectra of **1**, **2**, **RuP1**, **RuP2**, and **RuC** are shown in Fig. 3, and relevant data are collected in Table I. The absorption spectra of the complexes are dominated by metal-to-ligand charge-transfer (MLCT) transitions in the visible region and by ligand-centered (LC) bands in the UV region, as is common for Ru(II) polypyridine complexes.[6] Differential pulse voltammetry (DPV) (see the supplementary material) confirmed that **RuC** undergoes several oxidation processes at mild potentials, as already reported in the literature.[5] Model complexes **RuP1** and **RuP2** exhibit a single, monoelectronic, and reversible oxidation process at about +1.15 V vs Ag/AgCl. In multicomponent species **1** and **2,** several oxidation processes are present, which can be assigned to specific components, taking advantage of comparison with the model subunits. In particular, the oxidation processes at a potential less positive than +1.10 V are assigned to the catalytic subunits, whereas the oxidation process at about +1.15 V vs Ag/AgCl is assigned to the mono-electron oxidation of the photosensitizer unit. Relevant data are reported in Table II. The small differences between the oxidation potentials of the various processes in the separated species **RuP1**, **RuP2**, and **RuC** and in the supramolecular photocatalysts **1** and **2** confirm that the electronic interaction between the photosensitizer and catalytic subunits of **1** and **2** is

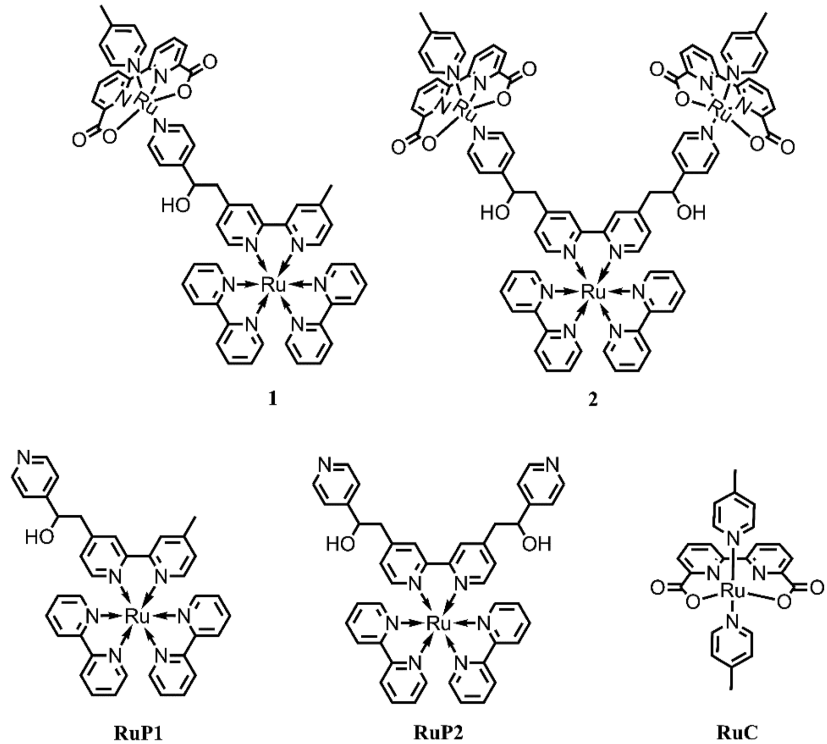

FIG. 1. Structural formulas of **1**, **2**, **RuP1**, **RuP2**, and **RuC**. Charges are omitted.

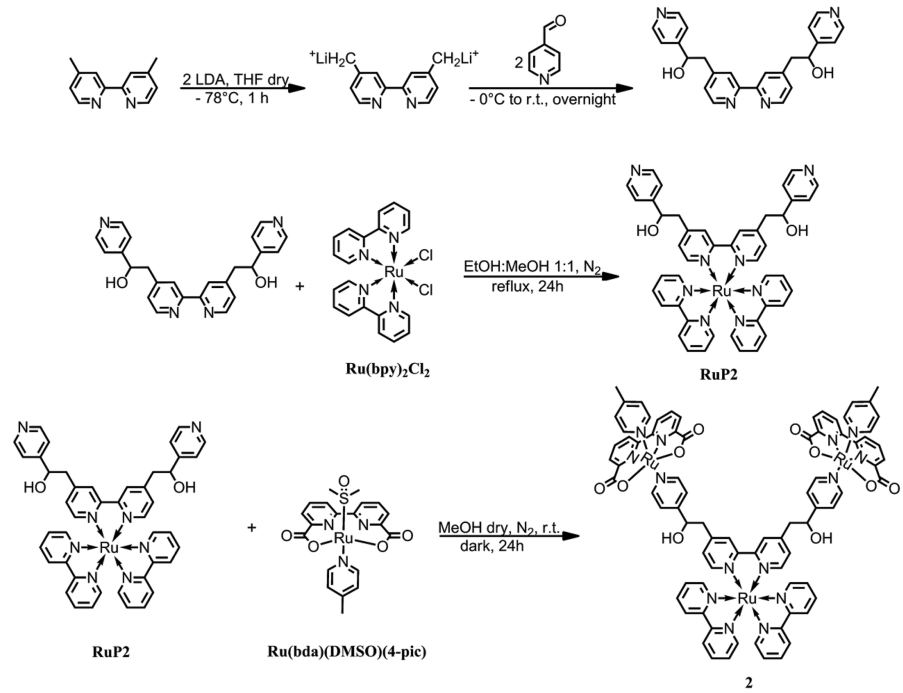

FIG. 2. Synthetic procedure for the preparation of **2**.

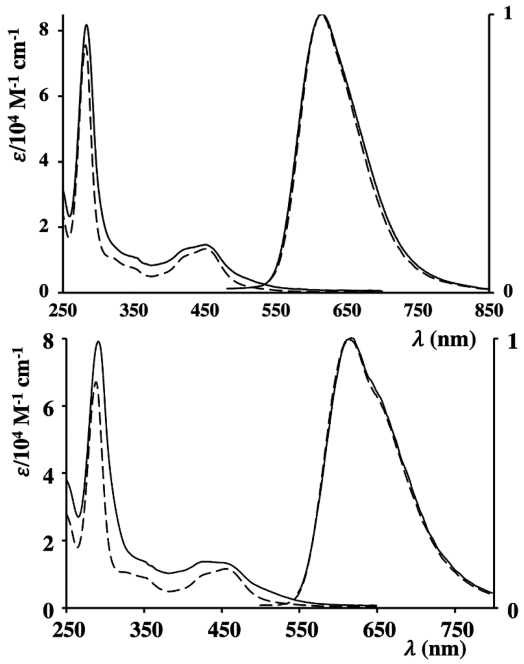

FIG. 3. Top panel: absorption and emission spectra of **RuP1** (dashed line) and **1** (solid line) in H_2O. Bottom panel: absorption and emission spectra of **RuP2** (dashed line) and **2** (solid line) in H_2O. Emission spectra are normalized.

TABLE I. Absorption spectra and photophysical properties in air-equilibrated water at room temperature.

	Absorption[a]		Luminescence	
	λ/nm (ε/M^{-1} cm^{-1})	λ/nm	φ	τ/ns
RuP1	450 (12 000)	613	0.024	405
RuP2	456 (11 600)	612	0.020	382
Ru(bpy)$_3$	452 (14 600)	620	0.028	500
1	450 (14 600)	613	0.007	76
2	430 (15 700)	612	0.002	53

[a]Maximum of the lowest-energy absorption band.

weak, which is the supramolecular nature of the multicomponent species.

RuP1, **RuP2**, **1**, and **2** exhibit the typical[3] MLCT emission of Ru(II) polypyridine complexes in aqueous solution (see relevant data in Table I and Fig. 3). However, both luminescence lifetimes and quantum yields of the multicomponent species **1** and **2** are significantly reduced in comparison with those of their model species, **RuP1** and **RuP2**, respectively, indicating that a quenching process is occurring. The rate constants of the quenching process are calculated according to Eq. (1), in which τ and τ_0 are the luminescence lifetimes of the multicomponent species and of the model compound, respectively, and k_q values are 1.1×10^7 s^{-1} for **1** and 1.6×10^7 s^{-1} for **2**. The larger quenching rate constant for **2** with

TABLE II. Oxidation potentials in buffer phosphate solution (pH 7.24, 40 mM) at room temperature. The concentration of the complexes is 0.4 mM. The reported oxidation potentials correspond to peaks in DPV experiments.

	E_{ox1}/V	E_{ox2}/V	E_{ox3}/V	E_{ox4}/V
RuP1	···	···	···	+1.07
RuP2	···	···	···	+1.14
1	+0.42	+0.70	+1.01	+1.08
2	+0.40	+0.74	+1.03	+1.18
$[Ru(bpy)_3]^{2+}$	···	···	···	+1.06
RuC	+0.47[a]	+0.71[a]	+1.05[a]	···

[a]Data reported in the mixed solvent MeCN/buffer phosphate.

respect to **1** is reasonable considering that in **2**, there are two potential quenchers,

$$k_q = 1/\tau - 1/\tau^0. \quad (1)$$

Emission quenching can be due to several processes. As reported for similar species, the driving force for energy transfer in both **1** and **2** is estimated to be around −0.30 eV (from the reported photoemission spectra at 77 K of a related photosensitizer and **RuC**, indicating that the excited-state energy of the photosensitizer is at about 2.05 eV and that of the catalytic species is at 1.75 eV).[8] The driving force for reductive photoinduced electron transfer for both **1** and **2** is estimated to be around −0.50 eV (see the supplementary material). Therefore, based on the luminescence data, no clear net information on the quenching process can be derived. In previously studied compounds,[8] emission quenching was mainly attributed to energy transfer. However, the connections between chromophore and catalysts in **1** and **2** are much larger than in the reported literature compounds,[8] in which the aliphatic $-CH_2-C(OH)H-$ spacers—which are part of the bridging ligands in **1** and **2**—are not present. This can definitely change the quenching mechanism since Dexter energy transfer (the dominant mechanism for energy transfer, as the Coulombic mechanism can be neglected in the present species) is usually slowed down more significantly than electron transfer with increasing distance.[4b,10] Investigation of the excited-state decay processes preceding photocatalysis would require ultrafast spectroscopy data, which are not available in our laboratory at the moment, so this issue is not faced here.

Chemical catalysis

The potential catalytic ability of **1** and **2** toward water oxidation was first examined from a chemical viewpoint, investigating the oxygen production in $HClO_4$ 0.1M (pH 1) in the presence of cerium ammonium nitrate (CAN, 200 mM) as the chemical oxidizing agent. Figure 4 shows the production of molecular oxygen with time at different concentrations of **1**, in the range of 5–35 μM, and that the

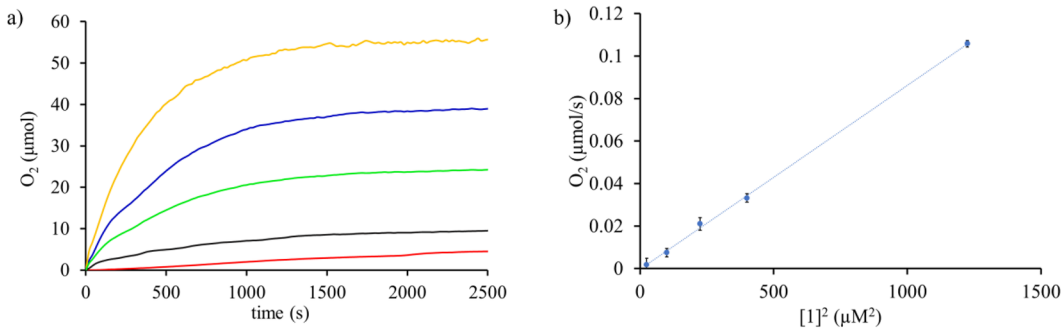

FIG. 4. (a) Kinetics of oxygen production vs time for **1** (5, 10, 20, and 35 μM; kinetic increases with catalyst concentration) in $HClO_4$ (0.1M, pH = 1) in the presence of CAN (200 mM) as a chemical oxidant. Detection of oxygen measurement: Ocean Optics oxygen sensor. (b) Initial rate of oxygen production vs $[\mathbf{1}]^2$, extracted from the first 50 s of the reaction; error bars denote the standard deviation of three experiments.

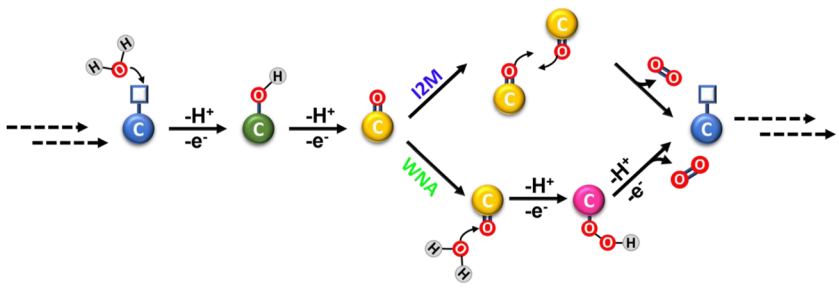

FIG. 5. Cartoon schematization of I2M and WNA mechanisms proposed for water oxidation. Different colors of the catalyst subunit indicate different oxidation states of the metallic catalytic center C (from blue, 2+, to pink, 5+).

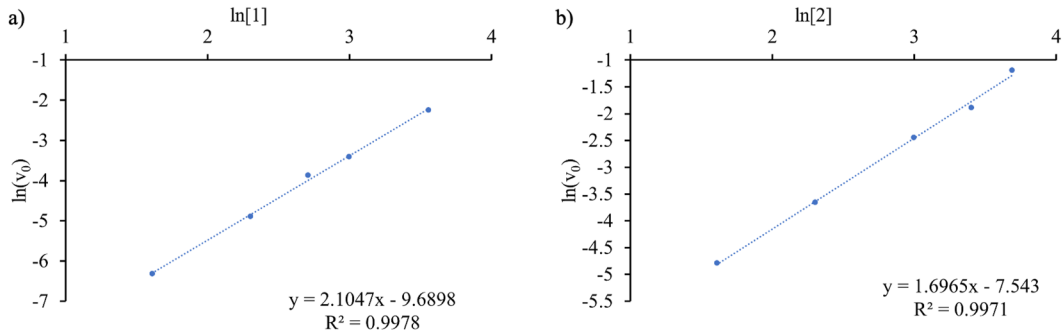

FIG. 6. ln(V_0) vs ln[CAT] for **1** (a) and **2** (b) in $HClO_4$ (0.1M, pH = 1) in the presence of CAN (200 mM) as a chemical oxidant.

oxygen production is linear with respect to the quadratic of the concentration of **1**. This latter result suggests the mechanism of water oxidation. Two main mechanisms, sometimes occurring simultaneously, are considered to be involved in water oxidation by molecular species.[11] The two mechanisms, water nucleophilic attack (WNA) and oxo–oxo coupling (I2M), particularly describe the pathway for O–O bond formation. A schematization is reported in Fig. 5. The main difference is that the I2M pathway requires the participation of two molecules, while WNA considers a nucleophilic attack on a single molecule. It has been proposed[12] that a clearcut differentiation between the mechanisms involved can be derived by the slope of the plot of ln(v_0) vs ln[catalyst], where v_0 is the concentration of the produced oxygen. As shown in Fig. 6, for **1**, this plot is linear with a slope of 2.1, a strong indication in favor of the I2M pathway, whose theoretical slope is 2. Further confirmation of the I2M pathway comes from analyzing the disappearance of the cerium ammonium nitrate absorption band at 360 nm as a function of the squared concentration of **1**. Assuming the I2M pathway, the initial rate constant of the process in **1** is 9.55×10^5 M^{-1} s^{-1} (see Fig. 7). Table III reports the turnover number (TON) and the turnover frequency (TOF) of **1** at different concentrations. The better results, under our experimental conditions, are obtained for higher concentrations of **1**, with a maximum TOF value of 0.75 s^{-1} obtained for 35 μM. However, it should be considered that, for technical reasons, the oxygen determination for a chemically driven process is performed in the space volume of the reactor, so a further process, equilibration between solution and space volume, could delay the determination of oxygen. The TOF values reported in Table III are, therefore, to be considered low limit values.

An intriguing result is also obtained by comparing the amount of molecular oxygen chemically produced by **1** and the model catalyst **RuC** (Fig. 8). Actually, Fig. 8 indicates that under the identical experimental conditions, the molecular oxygen produced by **RuC** stops after 150 s, whereas **1** (that had already produced a higher amount of oxygen than **RuC** within 150 s) continues to produce oxygen after 2500 s, resulting in a more than four-fold higher production of oxygen than **RuC** within 2500 s. This would suggest that the catalytic unit of **1** is more stable than **RuC** under catalytic conditions. Apparently, the presence of the covalently linked chromophore improves the stability of the catalytic subunit.

The production of molecular oxygen with time at different concentrations of **2**, in the range 5–40 μM, is shown in Fig. 9, which also shows that the oxygen production is linear for **2** with respect to the quadratic concentration of the catalyst. The slope of the plot of ln(v_0) vs ln[**2**] is 1.7 (see Fig. 6), suggesting that the main mechanism for water oxidation is I2M, also for **2**. A slightly higher rate constant for water oxidation, 2.69×10^6 M^{-1} s^{-1}, is found for **2** compared to **1** (see Fig. 10). The values of TON and TOF for the chemical oxidation of water by **2** are similar to those found for **1** (see Table III), with the

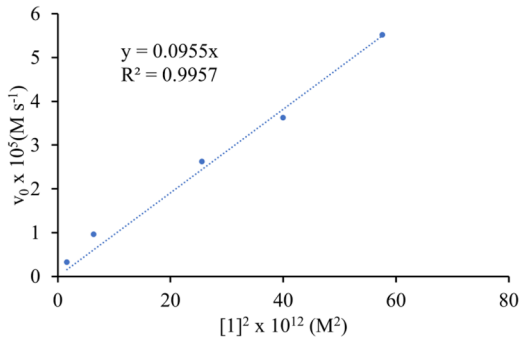

FIG. 7. Initial rate of consumption of CAN vs $[\mathbf{1}]^2$.

TABLE III. TON and TOF of **1** and **2** at different concentrations. The data in the table were calculated from experiments reported in Figs. 4 and 9.

[1] (μM)	TON	TOF (s^{-1})
5	334	0.09
10	353	0.19
20	502	0.42
35	423	0.75
[2] (μM)	TON	TOF (s^{-1})
5	165	0.21
10	262	0.32
20	287	0.54
40	343	0.95

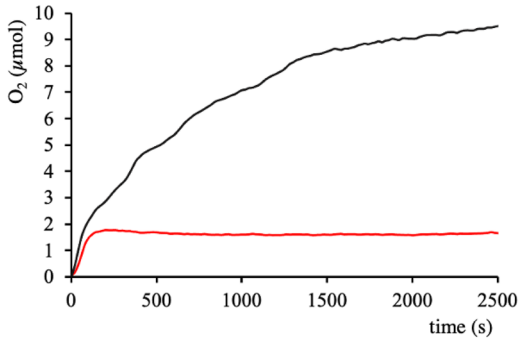

FIG. 8. Kinetic of oxygen production vs time for **1** (10 μM, black line) and **RuC** (10 μM, red line) in $HClO_4$ (0.1M, pH = 1) in the presence of CAN (200 mM) as a chemical oxidant. Detection of oxygen measurement: Ocean Optics oxygen sensor.

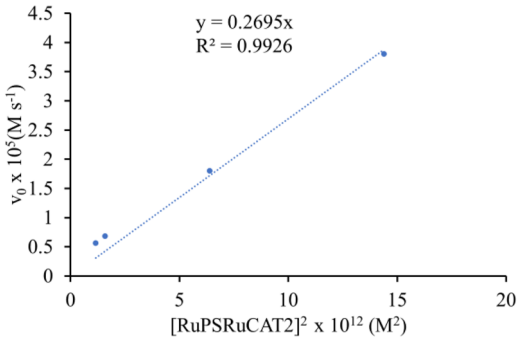

FIG. 10. Initial rate of consumption of CAN vs $[\mathbf{2}]^2$.

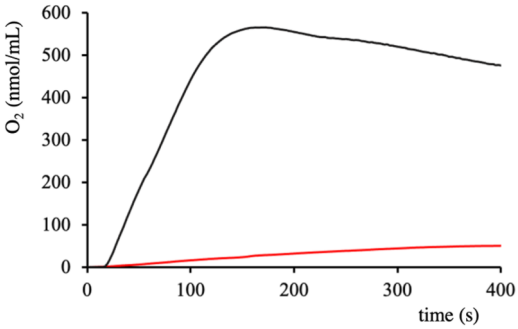

FIG. 11. Kinetic of oxygen production vs time for **2** (20 μM, black line) and **RuC** (40 μM, red line) in boric acid buffer 50 mM (pH = 7.24)/acetonitrile (10% of acetonitrile, v/v) in the presence of $Na_2S_2O_8$ (20 mM) as electron acceptor. In the experiment with **RuC** as a catalyst, $Ru(bpy)_3Cl_2$ (20 μM) as photosensitizer was used. Irradiation lamp, $\lambda > 400$ nm. Detection of oxygen measurement: Clark electrode.

better values obtained for the higher concentrations of **2** (e.g., 40 μM: 343 and 0.95 s^{-1} for TON and TOF, respectively).

Photocatalysis

In a typical experiment, a solution containing persulfate as the sacrificial agent (20 mM) in boric acid buffer (50 mM, pH 7.24) was degassed under nitrogen flow, and, after one hour and sensor calibration, the molecular photocatalyst at different concentrations was added. The mixture was irradiated with visible light ($\lambda > 400$ nm) using a xenon lamp with a cut-off filter, and the oxygen developed was measured using a Clark electrode for oxygen detection in solution. Full details are reported in the experimental section.

Figure 11 shows that molecular oxygen is produced using **2** as the supramolecular photocatalyst and persulfate as the sacrificial acceptor. The mechanism requires (i) oxidative quenching of the excited state of the chromophore by the sacrificial acceptor, followed by thermodynamically allowed hole transfer from the oxidized chromophore to the catalyst, or (ii) reductive quenching of the excited state of the chromophore by the catalyst subunit, followed by electron transfer from the reduced chromophore to the sacrificial agent; that is the "antibiomimetic" mechanism, already reported for dendritic chromophores.[13] The reduction of persulfate produces an even more efficient acceptor (sulfate anion radical), which can further drive the oxidation of the catalyst[1c,14] so that a single photon can

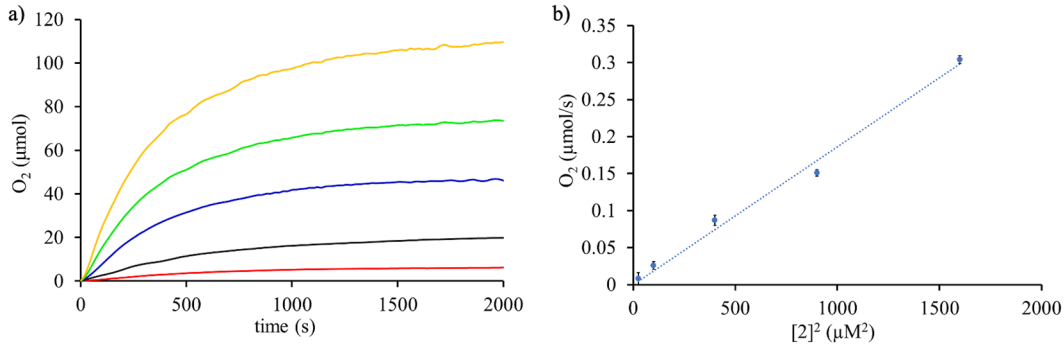

FIG. 9. (a) Kinetic of oxygen production vs time for **2** (5, 10, 20, and 40 μM; kinetic increases with catalyst concentration) in $HClO_4$ (0.1M, pH = 1) in the presence of CAN (200 mM) as a chemical oxidant. Detection of oxygen measurement: Ocean Optics oxygen sensor. (b) Initial rate of oxygen production vs $[\mathbf{2}]^2$, extracted from the first 50 s of the reaction; error bars denote the standard deviation of three experiments.

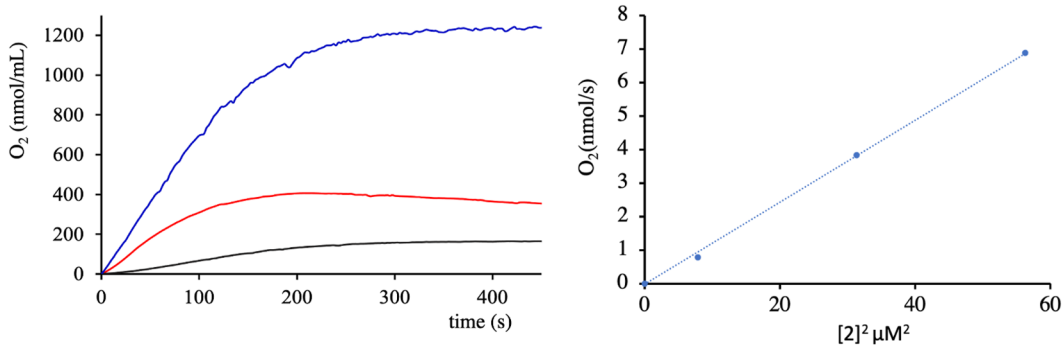

FIG. 12. Kinetic of oxygen production vs time for **2** (2.8, 5.6, and 7.5 μM; kinetic increases with catalyst concentration) in boric acid buffer 50 mM (pH = 7.24) in the presence of $Na_2S_2O_8$ (20 mM) as electron acceptor. Irradiation lamp, $\lambda > 400$ nm. Detection of oxygen measurement: Clark electrode.

drive two oxidation processes of the supramolecular photocatalyst. The experiments shown in Fig. 11 also clearly indicate that **2** is much more efficient for photoinduced water oxidation than a system made of separated $[Ru(bpy)_3]^{2+}$ and **RuC** (the concentration of the latter is twice compared to that of the chromophore, to simulate the chromophore:catalyst ratio in **2**). The experiments in Fig. 11 were performed in the presence of acetonitrile (10%) to allow the solubilization of **RuC**. Interestingly, on performing the same experiment for **2** in an aqueous solution (pH 7.24 for boric acid buffer), the amount of produced oxygen largely increases, making the determination by Clark electrode impossible because of saturation (see the supplementary material, Fig. S8). To overlap the saturation problem, it was needed to decrease the concentration of the supramolecular photocatalyst in a borate aqueous solution. To control whether the mechanism of water oxidation, even under photochemical irradiation, is I2M, such as for chemically driven catalysis, we performed photocatalysis at different concentrations. Figure 12, which reports as an example the results obtained for **2**, confirms that the catalytic mechanism for water oxidation is I2M even when the catalytic process is photochemically driven. Table IV reports the TON and TOF of **2** in photochemically driven catalysis, with the highest value obtained for the highest concentration (7.5 μM), which corresponds to a TOF of 1.22 s^{-1}. It could be noted that an apparent higher TOF value is found for the photocatalytic process (Table IV) than for the chemically driven process (Table III). However, it should be considered that the molecular oxygen produced upon a chemically driven experiment is, for technical reasons, determined in the space volume of the reactor, whereas the molecular oxygen photocatalytically produced is measured in solution. The determination of oxygen in the space volume of the reactor introduces another process, which is the equilibration between solution and space volume, so the determined oxygen production is delayed (see also above). In other words, the TOF values reported in Tables III and IV are not directly comparable.

TABLE IV. TON and TOF of **2** under photo-driven catalysis at different concentrations. The data in the table were calculated from photocatalytic experiments reported in Fig. 12.

[2] (μM)	TON	TOF (s^{-1})
2.8	29	0.35
5.6	35	0.85
7.5	83	1.22

The results in Fig. 13 indicate that supramolecular photocatalyst **2** produces about twice the amount of molecular oxygen produced by **1** under the same experimental conditions. At first sight, this could be attributed to the number of catalyst subunits in **2** compared to **1**. However, the overall concentration of catalyst subunits is identical, considering the relative concentrations of **1** and **2**, which balance the chromophore:catalyst ratio. This consideration tends to suggest a better efficiency of **2** compared to **1** for water oxidation. A possible explanation could assume a supramolecular organization of the supramolecular photocatalyst in the bimolecular assembly required for the I2M mechanism involved in the O–O formation bond, considered a rate limiting step for the whole catalytic process.[11] In fact, when a catalytically active site of **2** (which involves a highly oxidized metal site) interacts with a catalytic site of another molecule, the possible useful interactions with other catalytic units are twice as many as in the case of **1**, since the activated catalytic site can be hosted within the cavity formed by the two catalytic subunits of **2** (Fig. 14). In other words, increased local concentrations of

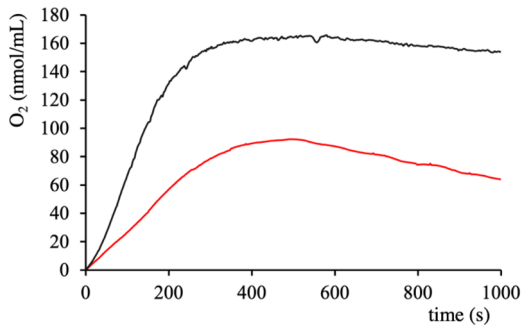

FIG. 13. Kinetic of oxygen production vs time for **1** (5.6 μM, red line) and **2** (2.8 μM, black line) in boric acid buffer 50 mM (pH = 7.24) in the presence of $Na_2S_2O_8$ (20 mM) as electron acceptor. Irradiation lamp, $\lambda > 400$ nm. Detection of oxygen measurement: Clark electrode.

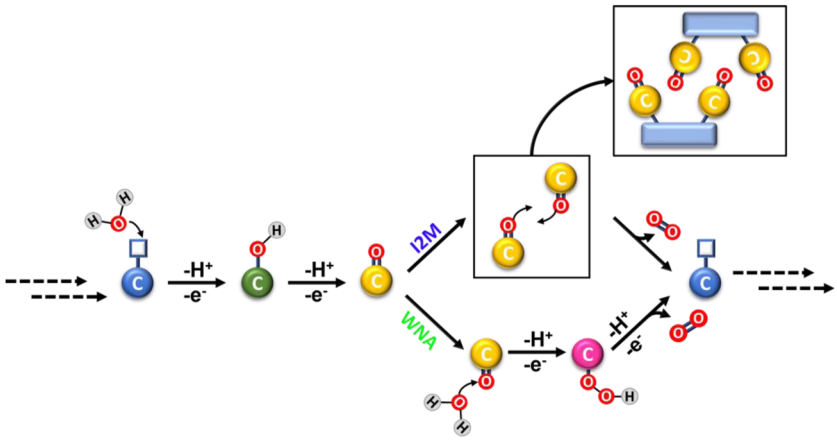

FIG. 14. Pathway of the I2M mechanism proposed for **2** (see squared figure).

catalytic subunits involved in the I2M mechanism could be at the origin of the improved efficiency of **2**. Interestingly, a higher rate for water oxidation was calculated for **2** in comparison with **1** for the chemically driven catalytic process (comparison between the data reported in Figs. 8 and 10), in agreement with the proposed mechanism.

CONCLUSIONS

Two new multicomponent supramolecular photocatalysts for water oxidation, **1** and **2**, have been prepared, together with their model chromophoric species **RuP1** and **RuP2**, and their chemically driven and photo-driven catalytic properties have been studied. The new supramolecular species **1** and **2** contain a $Ru(bpy)_3$-type chromophore covalently linked to one or two $[RuL(pic)_2]$ catalytic subunits, respectively. The typical MLCT emissions of the model compounds **RuP1** and **RuP2** are significantly quenched in the supramolecular species, with quenching rate constants of $1.1 \times 10^7\ s^{-1}$ for **1** and $1.6 \times 10^7\ s^{-1}$ for **2**. Both intramolecular energy and reductive electron transfer can be responsible for the emission quenching, but the effective mechanism cannot be determined with the present data.

Both **1** and **2** exhibit catalytic water oxidation in the presence of cerium ammonium nitrate, with an I2M mechanism, with catalytic efficiencies that are superior to those shown by the known catalyst $[RuL(pic)_2]$ under the same experimental conditions. Upon light irradiation, in the presence of persulfate as sacrificial acceptor agents, **1** and **2** are more efficient than a system made of separated $[Ru(bpy)_3]^{2+}$ and $[RuL(pic)_2]$ species, highlighting the advantage of using multicomponent, supramolecular species with respect to isolated species, in which electron transfer processes are slowed down owing to diffusion processes. Moreover, the photocatalytic process of **2** is more efficient than that of **1**. A possible reason could be an increased local concentration of catalytic subunits in the needed bimolecular assembly required for the I2M mechanism involved in the O–O formation bond for **2** with respect to **1**, as an effect of the presence of two catalytic subunits in the same multicomponent species **2**. No direct connection between the better photocatalytic efficiencies of the chromophore:catalyst subunit ratio 1:2 and the ratio 1:1 in the supramolecular photocatalysts previously reported as far as CO_2 photoreduction is concerned[9] is discussed, since the proposed reason in the case of CO_2 photoreduction would have a different origin.[9]

EXPERIMENTAL SECTION

General procedures

All solvents and chemicals were purchased from Merck and used as received. All reactions were performed in an inert atmosphere. 2,2′-bipyridine-6,6′-dicarboxylic acid (H_2bda),[15] 4-[2-(4-pyridyl)-2-hydroxyethyl]-4-methyl-2,2′-bipyridine (L1),[16] 4,4′-bis[2-(4-pyridyl)-2-hydroxyethyl]-2,2′-bipyridine (L2),[16] Ru(bda)$(DMSO)_2$,[17] Ru(bda)(DMSO)(pic),[18] Ru(bda)$(pic)_2$,[5] and $Ru(bpy)_2Cl_2$[19] were prepared as reported in the literature. ^{1}H NMR spectra were collected with a Varian 500 spectrometer operating at 500 MHZ in a deuterated solvent at room temperature. The chemical shift (δ), reported in ppm, refers to the residual solvent signal.

The UV–Vis absorption spectra were recorded with a JASCO V-560 spectrophotometer. The emission measurements were performed with a SpexJobin Yvon FluoroMax-2 spectrofluorometer equipped with a photomultiplier, Hamamatsu R3896. Emission quantum yields were calculated using $[Ru(bpy)_3]Cl_2$ in an aerated aqueous solution (Φ_{em} = 0.028)[20] as a reference. Emission lifetimes were performed with a time correlated single photon counting OB-900 spectrophotometer from Edinburg Instruments equipped with a 408 nm laser as an excitation light source.

Electrochemical measurements were performed using an Autolab multipurpose potentiostat with a GPES electrochemical interface in a three-electrode cell using as the working electrode an Amel glassy carbon (3 mm diameter), as the reference electrode an aqueous Ag/AgCl (3M KCl aqueous solution), and as the counter electrode a platinum wire. The supporting electrolyte used was the phosphate buffer (40 mM, pH 7.24).

The kinetic investigations were performed following the absorption decay at 360 nm of the Ce^{4+} consumption in an acidic aqueous solution ($HClO_4$ 0.1M). The catalyst was added to an acidic aqueous solution of cerium(IV) ammonium nitrate directly in a 3 ml cuvette located within the spectrophotometer compartment for immediate measurement. The Ce^{4+} absorption (ε_{360} = 380 M^{-1} cm^{-1}) was monitored over 1000 s.

The chemically driven water oxidation reactions were performed under ambient conditions. The oxygen evolution was measured using an Ocean Optics oxygen sensor (FOXY-OR125-G) with a multifrequency phase fluorometer (MFPF-100) connected to a computer. Over the probe tip, a Teflon membrane was installed before each experiment, as well as a two-point calibration with an oxygen free solution (purged with N_2 for one hour) and air saturated water. The calibration was adjusted to give a reading of 19% O_2 for air saturated water. In a typical measure, a concentrated solution of the catalysts was added to the cerium solution after one hour of bubbling N_2. The initial rates of oxygen evolution (μmol s^{-1}) were obtained by evaluating the slope of the plot of oxygen production vs time in the first 50 s.

For the photocatalysis experiment, a solution containing the sacrificial agent (20 mM) in boric acid buffer (50 mM, pH 7.24) was degassed under nitrogen flow, and, after one hour and sensor calibration, the molecular photocatalyst at different concentrations was added. The mixture was irradiated with visible light $\lambda > 400$ nm using a xenon lamp (Newport) with a cut-off filter at 400 nm, and the oxygen developed was measured using a Clark electrode (Oxygraph Plus Clark-electrode system from Hansatech) for oxygen detection in solution. The oxygen electrode disk is an electrochemical cell known as a Clark type polarographic sensor that comprises a resin bonded central platinum cathode and a concentric silver anode. The electrode disk is connected to a control unit, which supplies a polarizing voltage of 700 mV. In the presence of oxygen, a polarized disk generates a small current that is directly proportional to the concentration of oxygen in the reaction vessel above the cathode. This current is converted to a voltage, conditioned, and digitized with high resolution before being displayed by the electrode control unit. The system was calibrated in O_2-free (N_2 purge) and oxygen saturated (O_2 purge) water. The calibration was adjusted to give a reading of 19% O_2 for air saturated water. The mixture solution (2 ml) was purged with N_2 to provide an O_2-free solution. The OxyTrace+ software gave an O_2 reading every 2.5 s.

The pH of the solution after any photocatalytic experiment was checked. No changes with respect to the initial pH were recorded.

SUPPLEMENTARY MATERIAL

See the supplementary material for detailed synthesis and characterization [including nuclear magnetic resonance (NMR) spectra] of the new compounds, differential pulse voltammetry, and kinetics of photo-driven oxygen production vs time under various experimental conditions (Figs. S1–S9).

ACKNOWLEDGMENTS

This work was funded in part by a grant from the Italian Ministry of Foreign Affairs and International Cooperation (PGR project on artificial photosynthesis, collaboration Italy–Japan, Grant No. JP21GR09) and in part by the European Union (NextGeneration EU) through the MUR-PNRR Project SAMOTHRACE (Grant No. ECS00000022).

AUTHOR DECLARATIONS

Conflict of Interest

The authors have no conflicts to disclose.

Author Contributions

A.M.C., G.L.G., and S.C. conceived and coordinated the project. A.M.C., G.L.G., F.N., A.A., and M.G. performed the experimental investigation. All authors participated in discussing the data. A.M.C., G.L.G., and S.C. wrote and edited the manuscript.

Ambra M. Cancelliere: Conceptualization (equal); Investigation (equal); Writing – original draft (equal); Writing – review & editing (equal). **Antonino Arrigo**: Investigation (equal). **Maurilio Galletta**: Investigation (equal). **Francesco Nastasi**: Investigation (equal). **Sebastiano Campagna,**: Conceptualization (equal); Supervision (equal); Writing – original draft (equal); Writing – review & editing (equal). **Giuseppina La Ganga**: Conceptualization (equal); Data curation (equal); Investigation (equal); Writing – original draft (equal); Writing – review & editing (equal).

DATA AVAILABILITY

The data that support the findings of this study are available within the article and its supplementary material.

REFERENCES

[1] (a) Y. Jiang, F. Li, B. Zhang, X. Li, X. Wang, F. Huang, and L. Sun, Angew. Chem., Int. Ed. **52**, 3398 (2013); (b) M. Schulze, V. Kunz, P. Frischmann, and F. Würthner, Nat. Chem. **8**, 576 (2016); (c) F. Puntoriero, A. Sartorel, M. Orlandi, G. La Ganga, S. Serroni, M. Bonchio, F. Scandola, and S. Campagna, Coord. Chem. Rev. **255**, 2594 (2011); (d) D. L. Ashford, M. K. Gish, A. K. Vannucci, M. K. Brennaman, J. L. Templeton, J. M. Papanikolas, and T. J. Meyer, Chem. Rev. **115**, 13006 (2015); (e) T. J. Meyer, M. V. Sheridan, and B. D. Sherman, Chem. Soc. Rev. **46**, 6148 (2017); (f) D. K. Dogutan and D. G. Nocera, Acc. Chem. Res. **52**, 3143 (2019); (g) D. Wang, Z. Xu, M. V. Sheridan, J. J. Concepcion, F. Li, T. Lian, and T. J. Meyer, Chem. Sci. **12**, 14441 (2021).

[2] (a) J. D. Blakemore, R. H. Crabtree, and G. W. Brudvig, "Molecular catalysts for water oxidation," Chem. Rev. **115**, 12974 (2015); (b) A. Sartorel, M. Bonchio, S. Campagna, and F. Scandola, Chem. Soc. Rev. **42**, 2262 (2013); (c) L. L. Zhang, Y. Gao, Z. Liu, X. Ding, Z. Yu, and L. Sun, "A trinuclear ruthenium complex as a highly efficient molecular catalyst for water oxidation," Dalton Trans. **45**, 3814 (2016); (d) S. Piccinin and S. Fabris, Phys. Chem. Chem. Phys. **13**, 7666 (2011); (e) R. Matheu, P. Garrido-Barros, M. Gil-Sepulcre, M. Z. Ertem, X. Sala, C. Gimbert-Surinach, and A. Llobet, Nat. Rev. Chem **3**, 331 (2019); (f) P. Greife, M. Schönborn, M. Capone, R. Assuncao, D. Narzi, L. Guidoni, and H. Dau, Nature **617**, 623 (2023).

[3] (a) N. Kaveevivitchai, R. Chitta, R. Zong, M. El Ojaimi, and R. P. Thummel, J. Am. Chem. Soc. **134**, 10721 (2012); (b) P. Farràs, S. Maji, J. Benet-Buchholz, and A. Llobet, Chem. - Eur. J. **19**, 7162 (2013); (c) L. Zedler, A. K. Mengele, K. M. Ziems, Y. Zhang, M. Wächtler, S. Gräfe, T. Pascher, S. Rau, S. Kupfer, and B. Dietzek, Angew. Chem., Int. Ed. **58**, 13140 (2019).

[4] (a) V. Gray, K. Moth-Poulsen, B. Albinsson, and M. Abrahamsson, Coord. Chem. Rev. **362**, 54 (2018); (b) M. Natali and F. Scandola, in *Applied Photochemistry*, edited by G. Bergamini and S. Silvi (Springer, 2016), p. 1.

[5] L. Duan, A. Fischer, Y. Xu, and L. Sun, J. Am. Chem. Soc. **131**, 10397 (2009).

[6](a) T. J. Meyer, Pure Appl. Chem. **58**, 1193 (1986); (b) A. Juris, V. Balzani, F. Barigelletti, S. Campagna, P. Belser, and A. von Zelewsky, Coord. Chem. Rev. **84**, 85 (1988); (c) A. Arrigo, F. Nastasi, G. La Ganga, F. Puntoriero, G. Zappalà, A. Licciardello, M. Cavazzini, S. Quici, and S. Campagna, Chem. Phys. Lett. **683**, 96 (2017); (d) S. Campagna, F. Puntoriero, F. Nastasi, G. Bergamini, and V. Balzani, in *Photochemistry and Photophysics of Coordination Compounds I*, Topics in Current Chemistry Vol. 280 (Springer, 2007), p. 117.

[7](a) L. Duan, F. Bozoglian, S. Mandal, B. Stewart, T. Privalov, A. Llobet, and L. Sun, Nat. Chem. **4**, 418 (2012); (b) X. Zhou, F. Li, H. Li, B. Zhang, F. Yu, and L. Sun, ChemSusChem **7**, 2453 (2014); (c) Q. Chen, Q. Zhou, T.-T. Li, R. Liu, H. Li, F. Guo, and Y.-Q. Zheng, Transition Met. Chem. **44**, 349 (2019); (d) H. Li, F. Li, B. Zhang, X. Zhou, F. Yu, and L. Sun, J. Am. Chem. Soc. **137**, 4332 (2015); (e) F. L. Huber, A. M. Wernbacher, D. Perleth, D. Nauroozi, L. González, and S. Rau, Inorg. Chem. **60**, 13299 (2021); (f) M. G. Pfeffer *et al.*, Nat. Chem. **14**, 500 (2022); (g) J. Brückmann, C. Müller, T. Maisuradze, A. K. Mengele, D. Nauroozi, S. Fauth, A. Gruber, S. Gräfe, K. Leopold, S. Kupfer, B. Dietzek-Ivanšić, and S. Rau, Chem. - Eur. J. **28**, e2022007 (2022).

[8]L. Wang, M. Mirmohades, A. Brown, L. Duan, F. Li, Q. Daniel, R. Lomoth, L. Sun, and L. Hammarstrom, Inorg. Chem. **54**, 2742 (2015).

[9](a) A. M. Cancelliere, F. Puntoriero, S. Serroni, S. Campagna, Y. Tamaki, D. Saito, and O. Ishitani, Chem. Sci. **11**, 1556 (2020); (b) A. Santoro, A. M. Cancelliere, K. Kamogawa, S. Serroni, F. Puntoriero, Y. Tamaki, S. Campagna, and O. Ishitani, Sci. Rep. **13**, 11320 (2023).

[10]M. Natali, S. Campagna, and F. Scandola, Chem. Soc. Rev. **43**, 4005 (2014), and references therein.

[11]D. W. Shaffer, Y. Xie, and J. J. Concepcion, Chem. Soc. Rev. **46**, 6170 (2017).

[12]T. Liu, G. Li, N. Shen, L. Wang, B. J. J. Timmer, A. Kravchenko, S. Zhou, Y. Gao, Y. Yang, H. Yang, B. Xu, B. Zhang, M. S. G. Ahlquist, and L. Sun, Chem. - Eur. J. **28**, e2021045 (2022).

[13]M. Natali, F. Puntoriero, C. Chiorboli, G. La Ganga, A. Sartorel, M. Bonchio, S. Campagna, and F. Scandola, J. Phys. Chem. C **119**, 2371 (2015).

[14](a) A. Harriman, M. Richoux, P. A. Christensen, S. Mosseri, and P. Neta, J. Chem. Soc., Faraday Trans. 1 **83**, 3001 (1987); (b) M. Hara, C. C. Waraksa, J. T. Lean, B. A. Lewis, and T. E. Mallouk, J. Phys. Chem. A **104**, 5275 (2000); (c) P. G. Hoertz, Y. I. Kim, W. J. Youngblood, and T. E. Mallouk, J. Phys. Chem. B **111**, 6845 (2007).

[15]M. Y. Alyapyshev, V. A. Babain, N. E. Borisova, R. N. Kiseleva, D. V. Safronov, and M. D. Reshetova, Mendeleev Commun. **18**, 336 (2008).

[16]P. D. Beer, N. C. Fletcher, A. Grieve, J. W. Wheeler, C. P. Moore, and T. Wear, J. Chem. Soc., Perkin Trans. 2 **1996**, 1545.

[17]Y. Gao, X. Ding, J. Liu, L. Wang, Z. Lu, L. Li, and L. Sun, J. Am. Chem. Soc. **135**, 4219 (2013).

[18]B. D. Sherman, Y. Xie, M. V. Sheridan, D. Wang, D. W. Shaffer, T. J. Meyer, and J. J. Concepcion, ACS Energy Lett. **2**, 124 (2017).

[19]B. P. Sullivan, D. J. Salmon, and T. J. Meyer, Inorg. Chem. **17**, 3334 (1978).

[20]H. Ishida, S. Tobita, Y. Hasegawa, R. Katoh, and K. Nozaki, Coord. Chem. Rev. **254**, 2449 (2010).